



# Image decomposition based on the adaptive direction total variation and $\mathbb{G}$ -norm regularization

Baoli Shi<sup>1</sup> · Ge Meng<sup>2</sup> · Zhenjiang Zhao<sup>3</sup> · Zhi-Feng Pang<sup>1</sup>

Received: 28 January 2020 / Revised: 24 May 2020 / Accepted: 25 June 2020 / Published online: 16 July 2020  
© Springer-Verlag London Ltd., part of Springer Nature 2020

## Abstract

To improve the decomposition quality, it is very important to describe the local structure of the image in the proposed model. This fact motivates us to improve the Meyer's decomposition model via coupling one weighted matrix with one rotation matrix into the total variation norm. In the proposed model, the weighted matrix can be used to enhance the diffusion along with the tangent direction of the edge and the rotation matrix is used to make the difference operator couple with the coordinate system of the normal direction and the tangent direction efficiently. With these operations, our proposed model owns the advantage of the local adaption and also describes the image structure robustly. Since the proposed model has the splitting structure, we can employ the alternating direction method of multipliers to solve it. Furthermore, the convergence of the numerical method can be efficiently kept under the framework of this algorithm. Numerical results are presented to show that the proposed model can decompose better cartoon and texture components than other testing methods.

**Keywords** Image decomposition · Cartoon and texture · Alternating direction method of multipliers (ADMM) · Adaptive direction total variation regularization (ADTV) ·  $\mathbb{G}$ -norm

## 1 Introduction

Image decomposition plays an important role in the field of the computer vision. Let  $\Omega \subset \mathbb{R}^2$  to be the image domain, the target of the decomposition is of decomposing the image

---

This work was partially supported Hunan Provincial Key Laboratory of Mathematical Modeling and Analysis in Engineering (Changsha University of Science and Technology, China).

---

✉ Zhi-Feng Pang  
zhifengpang@163.com

Baoli Shi  
shibaoli1983@163.com

Ge Meng  
mengge1113@163.com

Zhenjiang Zhao  
zhaozhenjiang2009@163.com

- <sup>1</sup> College of Mathematics and Statistics, Henan University, Kaifeng 475004, Henan Province, China
- <sup>2</sup> Zhongyuan institute of statistics, Zhengzhou institute of finance and economics, Zhengzhou 450000, Henan Province, China
- <sup>3</sup> Department of Radiology, Luoyang Orthopedic Hospital of Henan Province, Zhengzhou 450018, Henan Province, China

$f : \Omega \rightarrow \mathbb{R}$  into two components as the cartoon  $u$  and the texture  $v$ , where  $u$  is formed by homogeneous regions with sharp boundaries and  $v$  is described to be the noise or small scale repeated details. Due to the lacking of some prior information, this problem is known to be an ill-posed problem. Therefore, some regularization techniques are usually imposed to minimize the following optimization problem

$$\begin{cases} \min_{u,v} R(u) + \lambda G(v), \\ \text{s.t. } f = u + v, \end{cases} \quad (1)$$

where the data fidelity term  $G(\cdot)$  depends on the degraded model, the regularization term  $R(\cdot)$  imposes the sparsity prior on the filter responses, and  $\lambda > 0$  is used to tune the contribution between  $R(\cdot)$  and  $G(\cdot)$ .

Model (1) is the classic decomposition model, and the choices of the terms  $R(\cdot)$  and  $G(\cdot)$  depend on the assignment of the image processing. For instance, in the image denoising,  $f$  is the noisy observed version of the true unknown image  $u$ , while  $v$  represents the additive noise. Often in this case, we can choose the total variation  $R(u) := \int_{\Omega} |\nabla u| dx$  [1] or the filtered variation  $R(u) := \int_{\Omega} |\mathbf{H}Du| dx$  [2] as the regularization term and  $G(v) := \frac{1}{2} \int_{\Omega} |v|^2 dx$  as the data fidelity

term. Here,  $\mathbf{D}$  and  $\mathbf{H}$  represent the signal transform (e.g., DCT, DHT, DFT) and the discrete-time filter in the transform domain, respectively. However, it has been pointed out in the seminal book [3] that the  $L^1$ -norm or  $L^2$ -norm does not characterize the oscillatory components. This means that these components do not have small norms. To the end, Meyer in [3] proposed to use the  $\mathbb{G}$ -norm, which is close to the weakly dual space of the bounded variation space  $\mathbb{BV}(\Omega)$ . So the model based on this norm can describe the oscillatory component in the image efficiently. However, due to its nonlinearity of the corresponding Euler–Lagrange equation, it is very difficult to get an exact numerical solution directly. Then, many modified decomposition models were proposed to overcome this difficulty. For example, Vese and Osher in [4] used a negative differentiability order  $\mathbb{W}^{1,p}(\Omega)$   $1 \leq p < \infty$  to approximate the  $\mathbb{G}$ -norm. Osher et al. in [5] proposed the  $\mathbb{BV} - \mathbb{H}^{-1}$  model, where the  $\mathbb{H}^{-1}$ -norm owns that its value is low for any high-frequency patterns and a large part of the noise. Aujol et al. in [6] made a modification to replace the  $\mathbb{G}$ -norm term by one constrained variable. In addition, some works based on the high-order total variation were also proposed for the decomposition problem [7–9]. However, the edges of objects in the resulting structure image decomposed by these aforementioned models are often blurred due to the fact that the model lacks the efficient description for the direction of the texture in the local region.

In this paper, we propose one novel direction-based model for better discriminating the cartoon component and texture component via coupling one weighted matrix with one rotation matrix into the TV norm. In the proposed model, the weighted matrix can be used to enhance the diffusion along with the tangent direction of the edge and the rotation matrix is used to make the difference operator couple with the coordinate system efficiently. With these operations, our proposed model owns the advantage of the local adaption and also describes the image structure robustly. Since the proposed model has the splitting structure, we can employ the alternating direction method of multipliers (ADMM) to solve it and the convergence can be kept in this algorithmic framework. Experimental results show that the proposed new model outperforms the state-of-the-art variational methods for the decomposition problem.

The remainder of this paper is organized as follows. Section 2 recalls some variation-based models related to our proposed model. Section 3 establishes our proposed model and also gives the numerical method to solve it. Experimental results and comparisons aiming at demonstrating the effectiveness of the proposed model are displayed in Sect. 4. Finally, concluding remarks are generalized in Sect. 5.

## 2 Related works

For the decomposition problem, many approaches were proposed based on how to model cartoon regions and texture patterns. Since this paper mainly considers to improve the variation-based models, we here recall some remarkable state-of-the-art models in order to establish foundations for image decomposition methodologies under the framework of the energy functional.

### 2.1 The $\mathbb{BVG}$ model

Since the space  $\mathbb{BV}(\Omega)$  can describe the piecewise constant region and also preserves image edge efficiently, many image decomposition models are proposed based on this space. However, this space is not suitable for describing the texture pattern. To this end, Meyer in [3] introduced the weakly dual form of the space  $\mathbb{BV}(\Omega)$  and then considered the following decomposition form

$$\begin{cases} \min_{u,v} J(u) + \lambda \|v\|_{\mathbb{G}}, \\ \text{s.t. } f = u + v, \end{cases} \quad (2)$$

where the  $\mathbb{BV}(\Omega)$  is defined the subspace of functions  $u \in L^1(\Omega)$  such that the following quantity is finite:

$$J(u) := \sup \left\{ \int_{\Omega} u \operatorname{div} \xi \, dx \mid \xi \in C_0^1(\Omega, \mathbb{R}^2), \|\xi\|_{L^\infty} \leq 1 \right\}$$

and the  $\mathbb{G}$ -norm is defined by

$$\begin{aligned} \|v\|_{\mathbb{G}} &= \inf_{\mathbf{g}} \left\{ \left\| \sqrt{g_1^2 + g_2^2} \right\|_{L^\infty} \mid \mathbf{g} \right. \\ &\quad \left. := (g_1, g_2) \in L^\infty(\Omega) \times L^\infty(\Omega) \right\} \end{aligned}$$

for  $v = \partial_1 g_1 + \partial_2 g_2 = \operatorname{div}(\mathbf{g})$  and  $\partial_1$  and  $\partial_2$  represent the subderivatives of  $g_1$  and  $g_2$ , respectively. In theory, this model can extract oscillatory components from the observation. However, it cannot be directly solved in practice due to the nonlinearity of the  $\mathbb{G}$ -norm. So some significant ideas were involved by using a duality argument [10] or the primal–dual scheme [11] to solve it.

### 2.2 The $\mathbb{BVH}^{-1}$ model

For the  $\mathbb{BVG}$  model, due to the impossibility of expressing its associated Euler–Lagrange equation, there exists a practical difficulty in numerical computation of getting the minimizer. One of the first attempts to overcome this difficulty has been made by Osher et al in [5], where they considered to approximate the  $\mathbb{G}$ -norm by its simplified version (called the  $\mathbb{BVH}^{-1}$  model)

$$\begin{cases} \min_{u,v} J(u) + \lambda \|v\|_{\mathbb{H}^{-1}(\Omega)}^2 \\ \text{s.t. } f = u + v. \end{cases} \quad (3)$$

Here, the function space  $\mathbb{H}^{-1}(\Omega)$  is dual form of the space  $\mathbb{H}_0^1(\Omega)$  and  $\|v\|_{\mathbb{H}^{-1}(\Omega)}^2 := \int_{\Omega} |\nabla(\Delta^{-1}v)|^2 dx$ . In general,  $\mathbb{H}^{-1}$ -norm owns that its value is low for any high-frequency patterns and a large part of the noise. In order to preserve the edges and contours of the image efficiently, Tang et al. in [12] extended model (3) to the nonconvex form by using the  $L^p$ -quasinorm ( $0 < p < 1$ ) to replace the  $L^1$ -norm for the  $\mathbb{BV}$ -semi-norm.

### 2.3 The $\mathbb{BV}$ -Gabor model

Though the  $\mathbb{BVH}^{-1}$  model is efficient to decompose the texture part and the cartoon part, it is not suitable for intermediate-frequency texture images decomposition. Accordingly, Aujol et al. in [13] introduce a convolution operator  $\mathbb{K}$  and its inverse  $\mathbb{K}^{-1}$ . In the proposed scheme,  $\mathbb{K}$  only penalizes frequencies that are not considered to be part of the texture component, so they were converted to  $\mathbb{K}^{-1}$ . The motivation is based on the fact that  $\mathbb{K}^{-1}$  can describe the frequencies included in the texture part. Above content can be implemented based on the Gabor functions. Specially, the  $\mathbb{BV}$ -Gabor ( $\mathbb{BVG}_A$ ) model can be written as

$$\min_u J(u) + \frac{\lambda}{2} \|\sqrt{\mathbb{K}}(f - u)\|_{L^2}^2. \quad (4)$$

The  $\mathbb{BVG}_A$  model is an appropriate approach to estimating the direction or frequency of a given texture image. Recently, Liu in [7] extended to replace the  $\mathbb{BV}$ -norm by the total generalized variation (TGV) in model (4) for the decomposition problem.

### 2.4 The $\mathbb{EHBV}$ model

As we known, the  $\mathbb{BV}$ -based models can lead to the staircase effect in the structure image [14]. An effective approach is to use the high-order bounded variation ( $\mathbb{HVB}$ ) to replace the  $\mathbb{BV}$ -norm in the proposed model. However, the  $\mathbb{HVB}$ -based models can blur object edges. Based on above facts, Duan et al. in [15] considered to couple the  $\mathbb{HVB}$  with the edge detection function  $\xi(\cdot)$  in order to preserve objects edge. Specifically, they proposed the following edge-weighted high-order bounded variation model ( $\mathbb{EHBV}$ ) as

$$\min_{u,\mathbf{g}} \frac{1}{2} \|f - u - \text{div}(\mathbf{g})\|_{L^2}^2 + \alpha \int_{\Omega} \xi(|\nabla f|) |\nabla^2 u| dx + \beta \int_{\Omega} \sqrt{g_1^2 + g_2^2} dx,$$

where  $|\nabla^2 u| = \sqrt{u_{xx}^2 + u_{xy}^2 + u_{yx}^2 + u_{yy}^2}$ ,  $\alpha$  controls the smoothness of the structure image  $u$ ,  $\beta$  determines how many

oscillations need to be kept in the texture component  $\text{div}(\mathbf{g})$ , and  $\mathbf{g} = (g_1, g_2) \in L^\infty(\Omega, \mathbb{R}^2)$ . The advantage of this model is that the computation efficiency has been dramatically improved and it also can preserve object edges due to the edge diffusivity function.

## 3 Adaptive direction $\mathbb{BV} - \mathbb{G}$ (ADBVG) decomposition model

Recently, many models by using the direction information were to overcome some drawbacks of the image restoration problem [16–19]. In fact, for the image decomposition, we also need the direction information to describe the texture parts. However, the aforementioned models in Sect. 2 based on the gradient information cannot describe these structures efficiently. In particular, for the numerical implementations, i.e., in the discrete space, the gradient operator only uses the horizontal or perpendicular direction. As a comparison, in the continuous space, the gradient operator depends on the directional derivative and then can point to the different direction. In order to offset these gaps between the discrete form and the continuous form, we need to add some direction information in the proposed model. To this end, we propose the decomposition model as follows:

$$\begin{cases} \min_{u,v} \int_{\Omega} |\mathbf{\Gamma}_\beta \mathbf{W}_{-\phi(f)} \nabla u| dx + \frac{\lambda}{2} \|f - u - v\|_{L^2}^2, \\ \text{s.t. } \|v\|_{\mathbb{G}} \leq \mu, \end{cases} \quad (5)$$

where  $\phi(f)$  denotes that the angle  $\phi$  depends on the original image  $f$ , and the rotation operator and the weighted operator are defined by

$$\mathbf{W}_{-\phi(f)} = \begin{bmatrix} \cos \phi(f) & \sin \phi(f) \\ -\sin \phi(f) & \cos \phi(f) \end{bmatrix} \quad \text{and} \quad \mathbf{\Gamma}_\beta = \begin{bmatrix} \beta & 0 \\ 0 & 1 \end{bmatrix} \quad (6)$$

for the weighted parameter  $\beta > 1$ . In practice, model (5) is difficult to be implemented due to the nature of the  $\mathbb{G}$ -norm. To this end, we employ the scheme used in [6,20] to transform the  $\mathbb{G}$ -norm to its dual form. We recall that the Legendre–Fenchel transform of the convex function  $F$  [21] is given by

$$F^*(v) = \sup_u \{ \langle u, v \rangle - F(u) \}.$$

Here,  $\langle \cdot, \cdot \rangle$  denotes the inner product in the space  $L^2(\Omega)$ . Set  $J(u) := F(u)$ , as did in [6,20], we can get

$$J^*\left(\frac{v}{\mu}\right) = \chi_{\mathbb{G}_\mu(\Omega)} = \begin{cases} 0 & \text{if } v \in \mathbb{G}_\mu(\Omega), \\ \infty & \text{otherwise,} \end{cases}$$

where

$$\mathbb{G}_\mu(\Omega) := \{v \in \mathbb{G}(\Omega) \text{ such that } \|v\|_{\mathbb{G}} \leq \mu\}.$$

With the help of above facts, we rewrite problem (5) into the following equivalent form

$$\min_{u,v} \int_{\Omega} |\Gamma_\beta \mathbf{W}_{-\phi(f)} \nabla u| dx + \frac{\lambda}{2} \|f - u - v\|_{L^2}^2 + J^* \left( \frac{v}{\mu} \right). \tag{7}$$

### 3.1 Numerical method

Here, we mainly consider the discrete case. The image is a two-dimensional vector of size  $M \times N$ . We denote by  $\mathbb{X}$  the Euclidean space  $\mathbb{R}^{M \times N}$  and  $\mathbb{Y} = \mathbb{X} \times \mathbb{X}$ . To the gradient operator  $\nabla \bar{u}$  for  $\bar{u} \in \mathbb{X}$  and the divergence operator  $\text{div} \widehat{\mathbf{g}}$  for  $\widehat{\mathbf{g}} \in \mathbb{Y}$ , we use the same notations as did in [22,23]. In addition, we denote the responding norms as

$$\|\bar{u}\|_2 := \sqrt{\sum_{i=1}^M \sum_{j=1}^N \bar{u}_{i,j}^2} \text{ and } \|\widehat{\mathbf{g}}\|_{2,1} = \sum_{i=1}^M \sum_{j=1}^N \sqrt{\sum_{s=1}^2 \widehat{\mathbf{g}}_{i,j,s}^2}.$$

Now we need to write problem (7) into the discrete form

$$\min_{u,v} \underbrace{\|\Gamma_\beta \mathbf{W}_{-\phi(f)} \nabla u\|_{2,1} + \frac{\lambda}{2} \|f - u - v\|_2^2 + J^* \left( \frac{v}{\mu} \right)}_{:= \mathcal{F}(u,v)}. \tag{8}$$

It is obvious that problem (8) is the multi-variational optimization problem, so we use the alternating direction method to minimize it with respect to  $u$  and  $v$  in an alternating fashion. To be specific, given some initial guess  $u^0$  and  $v^0$ , the simplest ADM solves the following two subproblems sequentially in each iteration:

$$\begin{cases} u^{n+1} = \operatorname{argmin}_u \mathcal{F}(u, v^n), \\ v^{n+1} = \operatorname{argmin}_v \mathcal{F}(u^{n+1}, v). \end{cases} \tag{9}$$

#### 3.1.1 Solving subproblem (9)

To minimize subproblem (9), one could directly solve its Euler–Lagrange equation. However, it is often controlled by the Courant–Friedrichs–Lewy (CFL) condition [24]. Based on the numerical optimization method, many works focused on the operator splitting method such as the primal–dual method [25], the dual-based method [26–28], the Douglas–Rachford method [29], and the alternating direction method of multipliers [30,31]. Here, we mainly use the ADMM to

solve subproblem (9). The ADMM was originally introduced in early 1970s [32,33] and has been studied extensively in the field of machine learning, computer vision, image and signal processing, and networking. The basic motivation of the ADMM is to first split the original nonsmooth minimization problem into several subproblems via introducing some auxiliary variables, and then solve each subproblem separately by employing some efficient numerical methods.

In order to use the ADMM to solve problem (9), we need to first transform it into an equivalent constrained optimization problem

$$\begin{cases} \min_{\mathbf{q}, \mathbf{p}, u} \frac{\lambda}{2} \|f - u - v^n\|_2^2 + \|\mathbf{q}\|_{2,1} \\ \text{s.t. } \mathbf{q} := (q_1, q_2)^T = \Gamma_\beta \mathbf{W}_{-\phi(f)} \mathbf{p} \\ \mathbf{p} := (p_1, p_2)^T = \nabla u \end{cases} \tag{11}$$

to decouple three linear operators  $\Gamma_\beta$ ,  $\mathbf{W}_{-\phi(f)}$  and  $\nabla$  away from the  $\|\cdot\|_{2,1}$  norm. Based on the augmented Lagrangian function, we then consider to solve the following saddle-point problem

$$\begin{aligned} \min_{\mathbf{q}, \mathbf{p}, u} \max_{\alpha, \eta} \mathcal{L}_{v^n}(\mathbf{q}, \mathbf{p}, u, \alpha, \eta) &= \frac{\lambda}{2} \|f - u - v^n\|_2^2 \\ &+ \|\mathbf{q}\|_{2,1} + \langle \alpha, \mathbf{p} - \nabla u \rangle + \frac{\gamma_1}{2} \|\mathbf{p} - \nabla u\|_2^2 \\ &+ \langle \eta, \mathbf{q} - \Gamma_\beta \mathbf{W}_{-\phi(f)} \mathbf{p} \rangle + \frac{\gamma_2}{2} \|\mathbf{q} - \Gamma_\beta \mathbf{W}_{-\phi(f)} \mathbf{p}\|_2^2, \end{aligned} \tag{12}$$

where  $\gamma_1$  and  $\gamma_2$  are the penalty parameters and  $\alpha := (\alpha_1, \alpha_2)^T$  and  $\eta := (\eta_1, \eta_2)^T$  are the Lagrange multipliers. Problem (12) includes five variables, so we need to solve one of the variables and simultaneously fix the others under the framework of the ADMM as shown in Algorithm 1.

Algorithm 1: ADMM to solve problem (11).

1. Input: original values of  $\mathbf{p}^0$ ,  $\alpha^0$  and  $\eta^0$ ;
2. Iterate (13)–(17) by
  - $\mathbf{q}^{k+1} := \operatorname{argmin}_{\mathbf{q}} \mathcal{L}_{v^n}(\mathbf{q}, \mathbf{p}^k, u^k, \alpha^k, \eta^k)$  (13)
  - $\mathbf{p}^{k+1} := \operatorname{argmin}_{\mathbf{p}} \mathcal{L}_{v^n}(\mathbf{q}^{k+1}, \mathbf{p}, u^k, \alpha^k, \eta^k)$  (14)
  - $u^{k+1} := \operatorname{argmin}_u \mathcal{L}_{v^n}(\mathbf{q}^{k+1}, \mathbf{p}^{k+1}, u, \alpha^k, \eta^k)$  (15)
  - $\alpha^{k+1} = \alpha^k + \gamma_1 (\mathbf{p}^{k+1} - \nabla u^{k+1})$  (16)
  - $\eta^{k+1} = \eta^k + \gamma_2 (\mathbf{q}^{k+1} - \Gamma_\beta \mathbf{W}_{-\phi(f)} \mathbf{p}^{k+1})$  (17)
 until stopping criterion is met.
3. Output:  $u := u^{k+1}$  as the cartoon image.

In the following, we consider to solve subproblems (13)–(17).

(1). **Subproblem q (13)**. This subproblem can be rewritten as

$$\mathbf{q}^{k+1} = \operatorname{argmin}_{\mathbf{q}} \|\mathbf{q}\|_{2,1} + \frac{\gamma_2}{2} \|\mathbf{q} - \mathbf{h}^k\|_2^2,$$

where  $\mathbf{h}^k := \left(\Gamma_\beta \mathbf{W}_{-\phi(f)} \mathbf{p}^k - \frac{\eta^k}{\gamma_2}\right)$ . It is the classic  $\ell_1 - \ell_2$  problem, so we can use the soft-thresholding operator to obtain closed-form solution as

$$\mathbf{q}^{k+1} = \max \left\{ 0, \left\| \mathbf{h}^k \right\|_{2,1} - \frac{1}{\gamma_2} \right\} \frac{\mathbf{h}^k}{\|\mathbf{h}^k\|_{2,1}}.$$

(2). **Subproblem p (14)**. It is a smooth and convex optimization problem, so its optimization condition can be written by

$$(\gamma_1 \mathcal{I} + \gamma_2 \mathbf{W}_{\phi(f)} \Gamma_\beta \Gamma_\beta \mathbf{W}_{-\phi(f)}) \mathbf{p}^{k+1} = \mathbf{b}^k,$$

where  $\mathcal{I}$  denotes a unit operator and

$$\mathbf{b}^k = \left(\gamma_1 \nabla u^k + \mathbf{W}_{\phi(f)} \Gamma_\beta \eta^k + \gamma_2 \mathbf{W}_{\phi(f)} \Gamma_\beta \mathbf{q}^{k+1} - \alpha^k\right).$$

With the simple computation, above linear equation system can be rearranged as

$$\begin{cases} a_{11} p_1^{k+1} + a_{12} p_2^{k+1} = b_1^k, \\ a_{21} p_1^{k+1} + a_{22} p_2^{k+1} = b_2^k, \end{cases} \tag{18}$$

where

$$\begin{aligned} a_{11} &:= \gamma_1 + \gamma_2(\beta^2 \cos^2 \phi(f) + \sin^2 \phi(f)), \\ a_{12} &:= a_{21} := \gamma_2(\beta^2 - 1) \sin \phi(f) \cos \phi(f), \\ a_{22} &:= \gamma_1 + \gamma_2(\beta^2 \sin^2 \phi(f) + \cos^2 \phi(f)), \\ b_1^k &:= \eta_1^k \beta \cos \phi(f) - \eta_2^k \sin \phi(f) - \alpha_1^k + \gamma_1 \nabla_x u^k \\ &\quad + \gamma_2 \left( q_1^{k+1} \beta \cos \phi(f) - q_2^{k+1} \sin \phi(f) \right), \\ b_2^k &:= \eta_1^k \beta \sin \phi(f) + \eta_2^k \cos \phi(f) - \alpha_2^k + \gamma_1 \nabla_y u^k \\ &\quad + \gamma_2 \left( q_1^{k+1} \beta \sin \phi(f) + q_2^{k+1} \cos \phi(f) \right). \end{aligned}$$

Since the coefficient matrix of equations (18) is non-singular, that is to say

$$\det(\gamma_1 \mathcal{I} + \gamma_2 \mathbf{W}_{\phi(f)} \Gamma_\beta \Gamma_\beta \mathbf{W}_{-\phi(f)}) \neq 0,$$

the solution  $\mathbf{p}^{k+1} = \left(p_1^{k+1}, p_2^{k+1}\right)^T$  can be obtained by using the Cramer’s rule as

$$\begin{cases} p_1^{k+1} = \frac{b_1^k a_{22} - b_2^k a_{12}}{a_{11} a_{22} - a_{12} a_{21}}, \\ p_2^{k+1} = \frac{b_2^k a_{11} - b_1^k a_{21}}{a_{11} a_{22} - a_{12} a_{21}}. \end{cases} \tag{19}$$

(3). **Subproblem u (15)**. Its minimizer is also determined by the corresponding Euler–Lagrange equation as follows:

$$(\lambda \mathcal{I} - \gamma_1 \Delta) u^{k+1} = \lambda (f - v^n) - \operatorname{div} \alpha^k - \gamma_1 \operatorname{div} \mathbf{p}^{k+1},$$

which is a linear elliptic equation with constant coefficients. With the assumption of the periodic boundary condition, we can use the fast Fourier transform (FFT) and its inverse transform to solve it via the following scheme

$$u^{k+1} = \mathcal{F}^{-1} \left( \frac{\mathcal{F}(\lambda (f - v^n) - \operatorname{div} \alpha^k - \gamma_1 \operatorname{div} \mathbf{p}^{k+1})}{\mathcal{F}(\lambda \mathcal{I} - \gamma_1 \Delta)} \right).$$

### 3.2 Solve the subproblem v in problem (10)

In order to solve problem (10), we use the same idea as did in [34], where the authors noticed that the solution can be obtained based on its dual argument. To this end, using the generalized Fermat rule, we can get

$$0 \in \partial \mathbb{F} \left( u^{n+1}, v \right), \tag{20}$$

where  $\partial(\cdot)$  denotes the Frechet differentiable. By using the dual theory [21]

$$g(x) \in \partial h^*(x) \Leftrightarrow h(x) \in \partial g(x).$$

and setting

$$w = \lambda (f - u^{n+1} - v),$$

then solving problem (20) is equivalent to solve

$$0 \in \operatorname{div} \left( \frac{\nabla w}{\|\nabla w\|_{2,1}} \right) - \frac{\lambda (f - u^{n+1}) - w}{\lambda \mu},$$

which is the Euler–Lagrangian equation of the optimization problem

$$\min_w \|\nabla w\|_{2,1} + \frac{1}{2\lambda\mu} \left\| \lambda f - \lambda u^{n+1} - w \right\|_2^2. \tag{21}$$

It is obvious that problem (21) is convex, nonsmooth and separable, so we can use the operator splitting scheme to transform it as the constrain optimization problem

$$\begin{cases} \min_{\mathbf{y}, w} \frac{1}{2\lambda\mu} \left\| \lambda f - \lambda u^{n+1} - w \right\|_2^2 + \|\mathbf{y}\|_{2,1}, \\ \text{s.t. } \mathbf{y} := (y_1, y_2)^T = \nabla w. \end{cases}$$



Furthermore, we obtain its corresponding saddle-point problem

$$\min_{\mathbf{y}, w} \max_{\boldsymbol{\theta}} \mathcal{L}_{u^{n+1}}(\mathbf{y}, w, \boldsymbol{\theta}, u) = \frac{1}{2\lambda\mu} \left\| \lambda f - \lambda u^{n+1} - w \right\|_2^2 + \|\mathbf{y}\|_{2,1} + \langle \boldsymbol{\theta}, \mathbf{y} - \nabla w \rangle + \frac{\gamma_3}{2} \|\mathbf{y} - \nabla w\|_2^2. \tag{22}$$

Then, similar to solve problem (9), we also use the ADMM to solve problem (22) as the following algorithm.

---

Algorithm 2: ADMM to solve problem (10).

---

1. Input: original values of  $\mathbf{y}^0, \boldsymbol{\theta}^0, \lambda$  and  $u^{k+1}$ ;
2. Iterate below until stopping criterion is met

$$\left\{ \begin{array}{l} \mathbf{y}^{k+1} := \max \left\{ 0, \left\| \nabla w^{t+1} - \frac{\boldsymbol{\theta}^t}{\gamma_3} \right\|_{2,1} - \frac{1}{\gamma_3} \right\} \frac{\nabla w^{t+1} - \frac{\boldsymbol{\theta}^t}{\gamma_3}}{\left\| \nabla w^{t+1} - \frac{\boldsymbol{\theta}^t}{\gamma_3} \right\|_{2,1}}, \\ w^{t+1} = \mathcal{F}^{-1} \left( \frac{\mathcal{F} \left( \frac{1}{\mu} (f - u^{n+1}) - \text{div} \boldsymbol{\theta}^t - \gamma_3 \text{div} \mathbf{y}^{t+1} \right)}{\mathcal{F} \left( \frac{1}{\lambda\mu} \mathcal{I} - \gamma_3 \Delta \right)} \right), \\ \boldsymbol{\theta}^{t+1} = \boldsymbol{\theta}^t + \gamma_3 \left( \mathbf{y}^{t+1} - \nabla w^{t+1} \right), \\ v^{t+1} = f - u^{n+1} - \frac{w^{t+1}}{\lambda}; \end{array} \right.$$

3. Output:  $v := v^{k+1}$  as the texture image.
- 

## 4 Numerical experiments

To illustrate the validity of our proposed model compared with other mentioned models as discussed in Sect. 2, this section presents a series of numerical comparisons to decompose the cartoon parts and texture parts from an image. However, for the image decomposition problem, we do not know the cartoon part  $\mathbf{u}$  and texture part  $\mathbf{v}$ , so how to describe the decomposition quality is very important. One of the efficient tools is to use the correlation to quantify it. This scheme was used in [13], where the authors assumed that the cartoon part and the texture part in an image are not correlated. Specially, they defined the correlation as

$$\text{Corr}(\mathbf{u}, \mathbf{v}) := \frac{\text{cov}(\mathbf{u}, \mathbf{v})}{\sqrt{\text{var}(\mathbf{u})\text{var}(\mathbf{v})}},$$

where  $\text{var}(\cdot)$  and  $\text{cov}(\cdot, \cdot)$  refer to the sample variance and the covariance of the given image respectively. Obviously, the small value of the Corr implies a better decomposition. Therefore, we use the *Corr* as the judgment standard for the decomposition result.

In model (5) or its equivalent form (8), the decomposition ability depends on how to choose the rotation angle  $\phi(f)$ . Since the orientation field estimation (OFE) used in the fingerprint recognition [35,36] can describe the direction of the

texture efficiently, we here employ it to estimate the angle  $\phi(f)$  in our numerical implementations. Specially, we first get one coarse orientation field by

$$o(f) = \frac{1}{2} \tan^{-1} \left( \frac{\sum_W 2\nabla_x f \cdot \nabla_y f}{\sum_W \left( (\nabla_x f)^2 - (\nabla_y f)^2 \right)} \right) + \frac{\pi}{2},$$

where  $W$  is a neighborhood window at the pixel point  $(i, j)$  for  $i = 1, \dots, M$  and  $j = 1, \dots, N^2$ . Then, we use the Gaussian smoothing function  $G_\sigma(f)$  to smooth  $o(f)$  via following scheme

$$\phi(f) = \frac{1}{2} \tan^{-1} \left\{ \frac{G_\sigma(f) * \sin(2 \cdot o(f))}{G_\sigma(f) * \cos(2 \cdot o(f))} \right\}$$

in order to weak the effect of the oscillation information in the texture part.

Besides the rotation angle  $\phi(f)$ , we also need to consider to how to choose the parameters  $\lambda$  and  $\mu$  in model (5), where they control the decomposition efficacy. Using the large values of  $\lambda$  and  $\mu$  will lead to remain more texture structures in the part of the cartoon, whereas the small values of them will make the part of the cartoon lost more structure. Therefore, these parameters need to be chosen cautiously for the given testing images. Here, we first fix the value of the parameter  $\mu$  and then tune the parameter  $\lambda$  by the trials and the errors. Specifically, we set the original value of  $\lambda$  into a bigger range as  $[a, b]$  and then find a suitable subset as  $[a_1, b_1] \subset [a, b]$  by the bisection method. In the next, we find a more suitable parameter in  $[a_i, b_i]$ . When the criteria values of the Corr and the structural similarity index (SSIM) are appropriate for composographs or the value of Corr is suitable for real images, we set this parameter as the chosen value of the parameter  $\lambda$ . In addition, we also notice that setting  $\beta \in [1.2, 3]$  can give a suitable decomposition result for the weighted matrix  $\Gamma_\beta$ . All experiments are performed using MATLAB(R2017a) on a windows(10)(64bit) desktop computer with an Intel core i7 2.40 GHz processor and 8.0GB of RAM.

### 4.1 Composographs

This section mainly considers to decompose two composographs as shown in Fig. 1, which are coupled together by the cartoon image  $\mathbf{u}$  and the texture image  $\mathbf{v}$ . Since the original images  $\mathbf{u}$  and  $\mathbf{v}$  are known, we can use the SSIM (structural similarity index) to quantify the efficiency of the decomposition besides the Corr. From Table 1, it is easy to observe that our proposed method performs the best in terms of both

<sup>2</sup> Here we set the  $W$  with the size  $16 \times 16$ .  $\tan^{-1}$  is the arctangent function with output range of  $(-\frac{\pi}{2}, \frac{\pi}{2})$

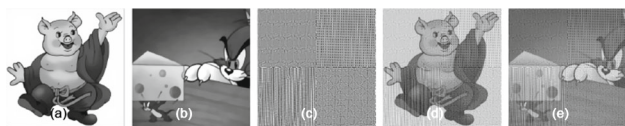


Fig. 1 a, b Cartoon image. c Texture image. d, e Composed image

Table 1 Corr(u, v) and SSIM based on different models

Image	Decomposition results of Fig. 1d				
	BVH <sup>-1</sup>	BVGA	EHBV	BVG	ADBGV
SSIM	0.7640	0.7510	0.8055	0.8742	<b>0.9159</b>
Corr	0.0644	0.0811	0.0284	0.0615	<b>0.0279</b>

Images	Decomposition results of Fig. 1e				
	BVH <sup>-1</sup>	BVGA	EHBV	BVG	ADBGV
SSIM	0.8924	0.9324	0.9441	0.9306	<b>0.9521</b>
Corr	0.0726	0.0713	0.0251	0.0364	<b>0.0217</b>

Best results are highlighted in bold font

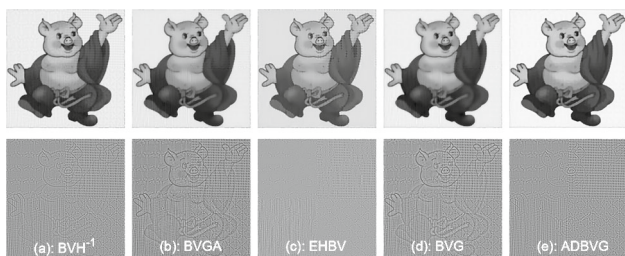


Fig. 2 Decomposition results by different models. Regularization parameters used in the models:  $[\lambda_{BVH^{-1}}, \lambda_{BVGA}, \lambda_{EHBV}, \lambda_{BVG}, (\lambda_{ADBGV}, \mu)] := [0.92, 0.37, 0.023, 620, (400, 0.2)]$

the SSIM and the Corr. In order to a better understand our proposed model, we show the decomposition results by different methods in Figs. 2 and 3. From Fig. 2, we can observe that there involves less cartoon information of our proposed model and the EHBV model than other models in the texture image. However, in the closeness of the cartoon part, our proposed model can preserve the edge more robust than other models, which can be observed from Figs. 2 and 3. In order to better describe these facts, we choose a part of the cartoon parts and then zoom them as shown in the left bottom of each image in Fig. 3. The ability to maintain image edges of our proposed can be obviously observed from the zoomed image. In addition, these facts can be also observed from the colorbars of the error images between the cartoon part in the original image and the cartoon part generated by the decomposition model, where the error image based on our proposed model is more dark than other models in Fig. 3. It actually implies that using our proposed model includes less details than other models in the cartoon components. In summary, both the visual inspection and quantitative evaluation have demonstrated the effectiveness of our proposed model.

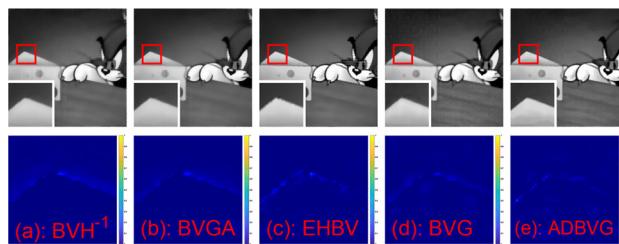


Fig. 3 Decomposition results by different models. The first row is the cartoon component. The second row is the visual comparison of the colorbar to the difference between the original cartoon component and the corresponding cartoon component of the decomposition results. Regularization parameters used in the models:  $[1.1, 0.31, 0.093, 520, (360, 0.26)]$

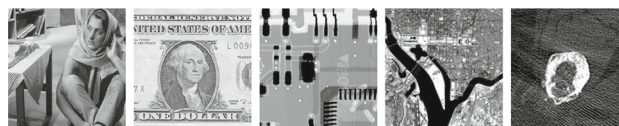


Fig. 4 Original images with the different size. From left to right: a Barbara (512 × 512), b Dollar (512 × 512), c circuit board (256 × 256), d band (256 × 256), e thighbone (256 × 256)

Table 2 Corr(u, v) based on the different model

Images	BVH <sup>-1</sup>	BVGA	EHBV	BVG	ADBGV
Barbara	0.0106	0.1181	0.0060	0.0169	<b>0.0037</b>
Dollar	0.0154	0.2083	0.0371	0.0630	<b>0.0115</b>
Board	0.0145	0.2246	0.0475	0.0650	<b>0.0036</b>
Band	0.0289	0.2194	0.0095	0.0459	<b>0.0016</b>
Thighbone	0.0202	0.0892	0.0045	0.0176	<b>0.0027</b>

Best results are highlighted in bold font

### 4.2 Real images

To more carefully compare our method with other methods, we consider to decompose five natural images and a CT image as shown in Fig. 4. In these images, (a)–(c) as the benchmark image are often used in the decomposition problem. Since the SSIM are not computable due to the unavailability of ground truths, we compare the results by the Corr as shown in Table 2. It is obvious that our model outperforms other models according to the Corr for all of the testing images. For the comparisons from the vision in Figs. 5, 6, and 7, we can see that our method is good at preserving the contour edges in cartoon component while rejecting them in the texture component. In order to compare these facts in detail, we also present the zoomed versions of the cartoon part and the texture part as shown in the bottom of Figs. 5, 6, and 7. It is easy to observe that the outputting of our proposed model tends to better separate them, with the sharp edges in the cartoon part and the clean texture information in the cartoon part.

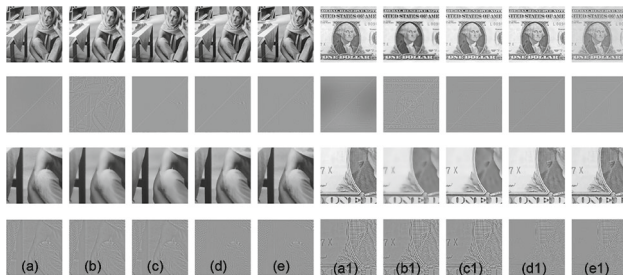


**Fig. 5** Decomposition results by different models. The bottom is the zoomed part of the cartoon and the texture. **a, a1**  $BVH^{-1}$ , **b, b1** BVGA, **c, c1** EHBV, **d, d1** BVG, **e, e1** ADBVG. Regularization parameters used in the models:  $[2,0.37,0.133,520,(440, 0.260)]$ (left);  $[0.9,0.4,0.123, 100,(160,0.2)]$  (right)

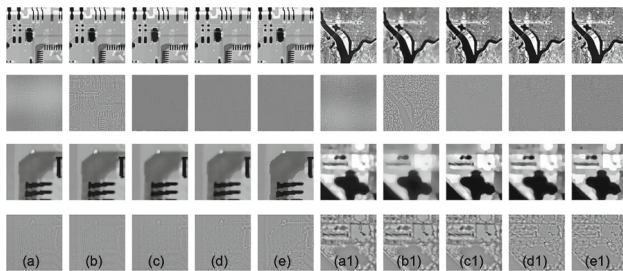


**Fig. 6** Decomposition results by different models. The bottom is the zoomed part of the cartoon and the texture. **a, a1**  $BVH^{-1}$ , **b, b1** BVGA, **c, c1** EHBV, **d, d1** BVG, **e, e1** ADBVG. Regularization parameters used in the models:  $[0.5,0.3,0.023,90,(100,0.4)]$ (left);  $[1.3,0.5,0.2, 150,(160,0.5)]$  (right)

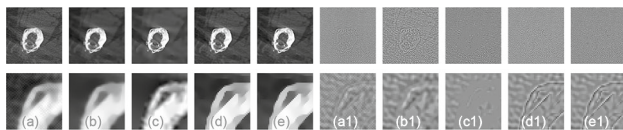


**Fig. 7** Decomposition results by different models. The bottom is the zoomed part of the cartoon and the texture. **a, a1**  $BVH^{-1}$ , **b, b1** BVGA, **c, c1** EHBV, **d, d1** BVG, **e, e1** ADBVG. The bottom is the zoomed part of the cartoon and the texture. Regularization parameters used in the models:  $[3.2,0.24,0.3,100,(80,0.5)]$

## 5 Conclusions

This paper proposed a new image decomposition model via combining the rotation matrix and the weighted matrix into the  $TV$  norm. In the proposed model, the weighted matrix can be used to enhance the diffusion along with the tangent direction of the edge and the rotation matrix is used to make the difference operator couple with the coordinate system of the normal direction and the tangent direction efficiently. With these operations, our proposed model owns the advantage of the local adaption and also describes the image structure robustly. Since the proposed model has the splitting structure, we can employ the alternating direction method of multipliers (ADMM) to solve it. Then, the convergence of

the numerical method can be efficiently kept. Experimental results reported the effectiveness of our proposed model.

## References

- Rudin, L., Osher, S., Fatemi, E.: Nonlinear total variation based noise removal algorithms. *Physica D* **60**(1–4), 259–268 (1992)
- Kose, K., Cevher, V., Cetin, A.: Filtered variation method for denoising and sparse signal processing. In: *IEEE International Conference on Acoustics, Speech and Signal Processing (ICASSP)*, pp. 3329–3332 (2012)
- Meyer, Y.: Oscillating patterns in image processing and nonlinear evolution equations. *Univ. Lect. Ser.* **22**, 1–123 (2001)
- Vese, L., Osher, S.: Modeling textures with total variation minimization and oscillating patterns in image processing. *J. Sci. Comput.* **19**(1–3), 553–572 (2003)
- Osher, S., Sole, A., Vese, L.: Image decomposition and restoration using total variation minimization and the  $H^{-1}$  norm. *Multiscale Model. Simul.* **1**(3), 349–370 (2003)
- Aujol, J., Aubert, G., Fraud, L., Chambolle, A.: Image decomposition into a bounded variation component and an oscillating component. *J. Math. Imaging Vis.* **22**(1), 71–88 (2005)
- Liu, X.: A new TGV-Gabor model for cartoon-texture image decomposition. *IEEE Signal Process. Lett.* **25**(8), 1121–1125 (2018)
- Gao, Y., Bredies, K.: Infimal convolution of oscillation total generalized variation for the recovery of images with structured texture. *SIAM J. Imaging Sci.* **11**(3), 2021–2063 (2018)
- Duan, J., Qiu, Z., Lu, W., Wang, G., Panc, Z., Bai, L.: An edge-weighted second order variational model for image decomposition. *Digit. Signal Process.* **49**, 162–181 (2016)
- Aujol, J., Chambolle, A.: Dual norms and image decomposition models. *Int. J. Comput. Vis.* **63**(1), 85–104 (2005)
- Wen, Y., Sun, H., Ng, M.: A primal-dual method for the Meyer model of cartoon and texture decomposition. *Numer. Linear Algebra Appl.* **26**(2), e2224 (2019)
- Tang, L., Zhang, H., He, C., Fang, Z.: Nonconvex and non-smooth variational decomposition for image restoration. *Appl. Math. Model.* **69**, 355–377 (2019)
- Aujo, J., Gilboa, G., Chan, T., Osher, S.: Structure-texture image decomposition modeling, algorithms, and parameter selection. *Int. J. Comput. Vis.* **67**(1), 111–136 (2006)
- Jalalzai, K.: Some remarks on the staircasing phenomenon in total variation-based image denoising. *J. Math. Imaging Vis.* **54**(2), 256–268 (2016)
- Duan, J., Lu, W., Pan, Z., Bai, L.: An edge-weighted second order variational model for image decomposition. *Digit. Signal Process.* **49**, 162–181 (2006)
- Bayram, I., Kamasak, M.: Directional total variation. *IEEE Signal Process. Lett.* **19**(12), 781–784 (2012)
- Kongskov, R., Dong, Y.: Directional total generalized variation regularization for impulse noise removal. In: *Scale Space and Variational Methods in Computer Vision*, pp. 221–231 (2017)
- Kongskov, R., Dong, Y., Knudsen, K.: Directional total generalized variation regularization. *BIT Numer. Math.* **59**(4), 903–928 (2019)
- Parisotto, S., Calatroni, L., Caliani, M., Schonlieb, C., Weickert, J.: Anisotropic osmosis filtering for shadow removal in images. *Inverse Probl.* **35**(5), 54001 (2019)
- Aujol, J., Kang, S.: Color image decomposition and restoration. *J. Vis. Commun. Image Represent.* **17**(4), 916–928 (2006)
- Rockafellar, R.: *Convex Analysis*. Princeton University Press, Princeton (2015)



22. Wu, C., Tai, X.: Augmented Lagrangian method, dual methods, and split Bregman iteration for ROF, vectorial TV, and high order models. *SIAM J. Imaging Sci.* **3**(3), 300–339 (2010)
23. Lu, W., Duan, J., Qiu, Z., Pan, Z., Liu, W., Bai, L.: Implementation of high order variational models made easy for image processing. *Math. Methods Appl. Sci.* **39**(14), 4208–4233 (2016)
24. Moura, C., Kubrusly, C.: *The Courant–Friedrichs–Lewy (CFL) Condition: 80 Years After Its Discovery*. Birkhauser, Basel (2013)
25. Chambolle, A., Pock, T.: A first-order primal-dual algorithm for convex problems with applications to imaging. *J. Math. Imaging Vis.* **40**(1), 120–145 (2011)
26. Chambolle, A.: An algorithm for total variation minimization and applications. *J. Math. Imaging Vis.* **20**(1–2), 89–97 (2004)
27. Aujol, J.: Some first-order algorithms for total variation based image restoration. *J. Math. Imaging Vis.* **34**(3), 307–327 (2007)
28. Bresson, X., Chan, T.: Fast dual minimization of the vectorial total variation norm and applications to color image processing. *Inverse Probl. Imaging* **2**(4), 455–484 (2008)
29. Steidl, G., Teuber, T.: Removing multiplicative noise by Douglas–Rachford splitting methods. *J. Math. Imaging Vis.* **36**(2), 168–184 (2010)
30. Wu, C., Zhang, J., Tai, X.: Augmented Lagrangian method for total variation restoration with non-quadratic fidelity. *Inverse Probl. Imaging* **5**(1), 237–261 (2011)
31. Zhang, J., Chen, R., Deng, C., Wang, S.: Fast linearized augmented method for Euler’s elastica model. *Numer. Math.: Theory Methods Appl.* **10**(1), 98–115 (2017)
32. Gabay, D., Mercier, B.: A dual algorithm for the solution of nonlinear variational problems via finite element approximation. *Comput. Math. Appl.* **2**(1), 17–40 (1976)
33. Glowinski, R., Marroco, A.: Sur l’approximation, par éléments finis d’ordre un, et la résolution, par dualité-dualité, d’une classe de problèmes de Dirichlet non linéaires. *Rev. Française d’Autom. Inf. Recherche Operationelle* **9**(R–2), 41–76 (1975)
34. Gilles, J., Osher, S.: Bregman implementation of Meyer’s G-norm for cartoon+textures decomposition. *UCLA cam*, 11–73 (2011)
35. Yang, G., Burger, P., Firmin, D., Underwood, S.: Structure adaptive anisotropic image filtering. *Image Vis. Comput.* **14**(2), 135–145 (1996)
36. Hong, L., Wan, Y., Jain, A.: Fingerprint image enhancement: algorithm and performance evaluation. *IEEE Trans. Pattern Anal. Mach. Intell.* **20**(8), 777–789 (1998)

**Publisher’s Note** Springer Nature remains neutral with regard to jurisdictional claims in published maps and institutional affiliations.